J. Fluid Mech. (1972), *vol.* 54, *part* 2, *pp.* 297–304
Printed in Great Britain

Strong shock propagation through decreasing density

By D. A. FREIWALD
Sandia Laboratories, Albuquerque, New Mexico

(Received 13 July 1971 and in revised form 13 March 1972)

The acceleration of a shock wave in an ideal gas of decreasing density has previously been studied. The problem is reconsidered here with empirical inclusion of real-gas effects for strong shocks in hydrogen. Experimental results suggest that previous shock acceleration models are valid only for a limited range of the Knudsen number in finite geometries and that for large final-state Knudsen numbers a free-expansion model best describes the experimental results.

1. Introduction

Nicholl (1951) and Gould (1952) investigated both experimentally and theoretically the interaction of weak shock waves with rarefaction waves in air in a wave interaction tube. This work has been summarized by Glass & Hall (1959). Zeldovich & Raizer (1967) treated the propagation of a shock for a power-law decrease in ambient gas density using similarity analysis. Stefanik (1969) has treated the problem for an ideal gas using perturbation techniques, as have Strachan, Huni & Ahlborn (1970), who formulated an expression describing the shock trajectory for varying ideal-gas pressure, density and particle velocity ahead of the shock and showed agreement between theory and experiments using reflected pure detonation waves. Greenspan & Butler (1962) considered theoretically the interaction of a plane infinite ideal gas shock with a complete centred rarefaction and predicted infinite shock acceleration in the vacuum region. Gurevich & Rumyantsev (1970) have investigated the stability of shocks propagating into a gas of decreasing density.

The problem considered here is the interaction of a strong laboratory shock with a density gradient in a real gas (having thermophysical properties): hydrogen. The problem is treated experimentally and theoretically and includes the case for which the Knudsen number is large in the final state. Explosively driven gradient shock tubes were used in the experiments. The theoretical framework was drawn from the work of Nicholl and Gould since this could easily be adapted for use with the real-gas equilibrium normal-shock calculations of Freeman (1968).

2. Theory

The essential phenomena are depicted schematically in figure 1, where P is pressure, ρ is density, t is time and x and ξ are distance. A rarefaction wave is created by opening a diaphragm separating the high and low pressure sections of

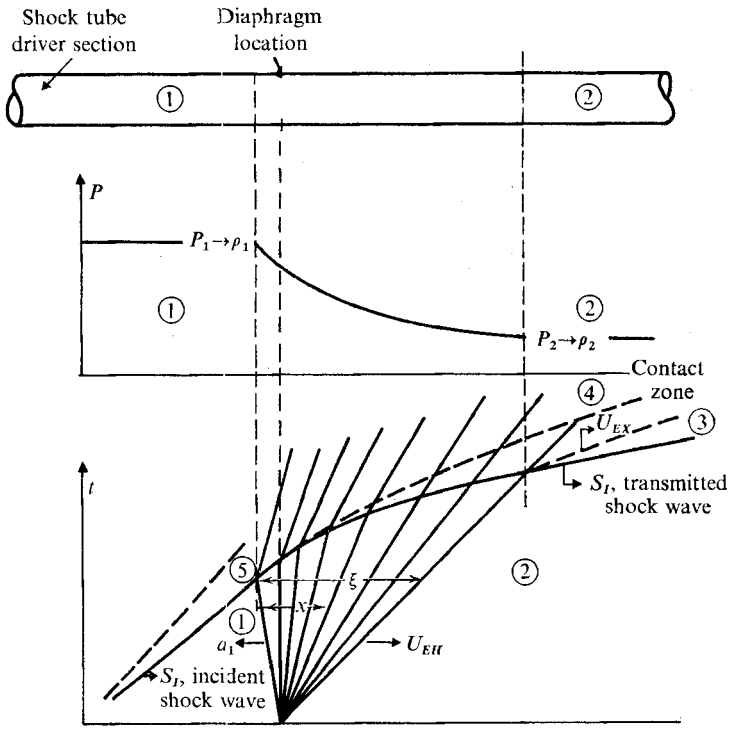

FIGURE 1. Shock–gradient interaction with sufficient upstream gas density.

the shock tube prior to arrival of the incident shock. A density gradient exists across this rarefaction wave. As the incident shock, travelling at speed S_I, propagates into the gradient it accelerates. We postulate that in a finite geometry one of two models will describe the transmitted flow in region 2.

Model 1

In this model we assume that there is sufficient gas in region 2 to support a well-structured transmitted shock of speed S_T. The following formulae then give the relationship between the various pressure ratios for the interaction of a shock wave and a rarefaction wave in an ideal gas with constant γ (= ratio of specific heats):

$$P_{32} = 1 + (1+\alpha_1 P_{32})^{\frac{1}{2}}\{D - E[(P_{32}P_{15})^{1/(\alpha_1+1)} - (P_{12})^{1/(\alpha_1+1)}]\}, \tag{1}$$

where

$$D = P_{12}^{1/(\alpha_1+1)}\frac{P_{51}-1}{(1+\alpha_1 P_{51})^{\frac{1}{2}}} + (\alpha_1+1)^{\frac{1}{2}}[1 - P_{12}^{1/(\alpha_1+1)}],$$

$$E = (\alpha_1+1)^{\frac{1}{2}}\{P_{51}[(\alpha_1+P_{51})/(1+\alpha_1 P_{51})]\}^{\frac{1}{2}},$$

$$\alpha_1 = (\gamma_1+1)/(\gamma_1-1).$$

Also, $P_{ij} = P_i/P_j$; a similar use of subscripts for ratios of densities will be employed.

Though (1) was derived with the implicit assumption of constant γ, one can show that real-gas effects only slightly modify the shock pressure ratios, which are determined mainly by the shock speed and initial density, as was discussed by

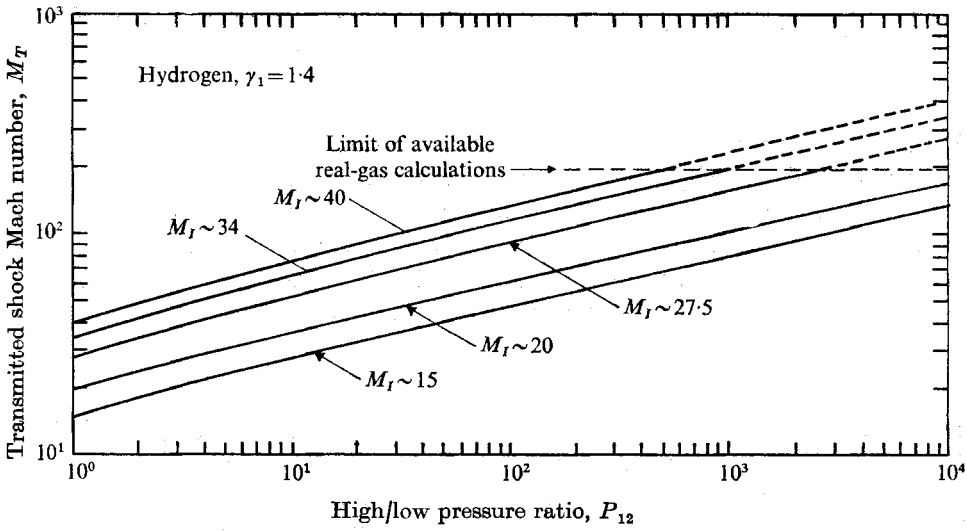

FIGURE 2. Calculated values for transmitted shock Mach number *vs.* gradient pressure ratio for various incident shock Mach numbers.

Gaydon & Hurle (1963). Using $\gamma_1 = 1{\cdot}4$ we have $\alpha_1 = 6$, and for strong shocks, namely, for $P_{51} > 100$, equation (1) reduces to

$$P_{32}^{\frac{1}{7}} = 3{\cdot}646P_{51}^{\frac{1}{7}} - 6{\cdot}481P_{12}^{\frac{1}{7}} + 6{\cdot}481 - 2{\cdot}646P_{51}^{\frac{5}{14}}P_{32}^{\frac{1}{7}}. \tag{2}$$

Equation (2) has been solved numerically, solutions being obtained as follows. For an incident shock Mach number $M_I = S_I/a$, where a is the pre-shock sound speed, the corresponding incident shock pressure ratio P_{51} was obtained from real-gas normal-shock calculations. For selected values of rarefaction wave pressure ratio P_{12}, the transmitted shock wave pressure ratio P_{32} was calculated from (2). The pressure ratio P_{32} was then converted to a transmitted shock Mach number $M_T = S_T/a$, again using real-gas normal-shock calculations. The results are shown in figure 2. It was assumed that shock precursors are unimportant and that the ambient gas sound speed maintains its ideal-gas value. Boundary-layer effects, stability considerations and shock curvature have been neglected.

When the Knudsen number on the low pressure side of the rarefaction wave is large, model 1 analysis is not expected to be valid. Instead, a transition from shock flow to free expansion is expected to occur within the gradient as the well-structured shock dissipates. For analysis purposes, it is thus necessary to know the pre-shock density profile in the rarefaction fan. The density profile is obtained using the formulae of Glass & Hall (1959). Assuming $P_{12} \gg 1$ gives the following formula for the density at any position x in a complete centred rarefaction wave of axial extent ξ:

$$\rho_x = \rho_1(1 - x/\xi)^{2/(\gamma_1 - 1)}. \tag{3}$$

The axial extent ξ as indicated in figure 1 is obtained from an $x - t$ wave diagram where the speed of the rarefaction wave head RH propagating into the high

pressure section is given by the local speed of sound a_1. The speed U_{EH} of the free expansion head is given by Greenspan & Butler (1962):

$$U_{EH} = [2/(\gamma_1 - 1)]a_1. \tag{4}$$

When ξ and the rarefaction wave density profile are known, using the mean-free-path data of McDaniel (1964) one can calculate the Knudsen number throughout the rarefaction wave as a function of x. If the Knudsen number at some position x or in region 2 is small, model 1 theory should apply there. If the Knudsen number becomes large in some region, it is postulated that model 1 will apply only up to that region, and that beyond it model 2 applies.

Model 2

In this model we assume that the density in region 2 is small in the sense that the Knudsen number Kn, the ratio of the mean free path λ to a characteristic length d, is too large to support a well-structured shock, i.e. that the shock thickness becomes comparable to the tube diameter, and boundary-layer effects sufficiently degrade the shock structure such that the shock jump formulae are no longer valid. Degradation of shock flow due to boundary layers at low pre-shock pressures has been discussed by Mirels (1963); shock thicknesses in hydrogen have been studied by Gross (1967). In model 2 we postulate that the shock 'dissipates' because of the wall effects and that the flow becomes a high-speed free expansion of speed U_{EX} in the low pressure region. The speed U_{EX} of the front of the expansion is obtained by adding the incident-shock flow speed to the expansion head speed of an initially quiescent gas:

$$U_{EX} = U_5 + \frac{2}{\gamma_5 - 1} a_5, \tag{5}$$

where it is to be noted that the incident post-shock sound speed a_5 and specific heats ratio γ_5 are used. Thus, though (1) is not sensitive to incident-shock real-gas effects, (5) is, through γ_5, which is obtained from the real-gas normal-shock calculations.

Equation (5) results from a simple superposition of the expansion head speed for the expansion of a gas into a vacuum and the flow speed U_5 established by the incident shock. Such simple superposition is not generally valid owing to the nonlinear nature of the underlying differential equations. However, this is a characteristic equation for a simple wave, and it will be seen that this model adequately describes the experiments. Using $a = (\gamma RT)^{\frac{1}{2}}$ and $U_5 \simeq 2S_I/(\gamma_1 + 1)$, (5) becomes

$$U_{EX} \simeq \tfrac{5}{6} S_I + \frac{2}{\gamma_1 - 1} \left(\frac{\gamma_5 T_5}{\gamma_1 T_1}\right)^{\frac{1}{2}} a_1. \tag{6}$$

In both model 1 and 2 above, the flow velocity induced by the centred rarefaction wave is neglected since one can show that for the strong shocks considered here the small pre-shock flow velocity in the gradient is at least an order of magnitude less than that induced by the shock. Obviously, a transition region will exist between the mathematical limits of model 1 and model 2.

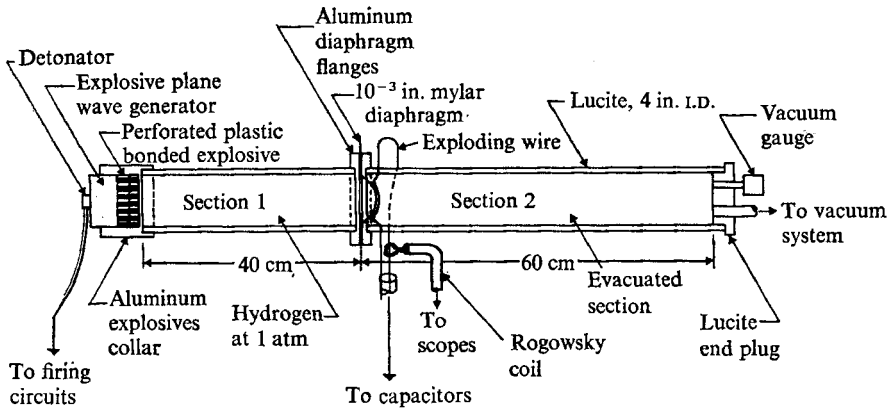

FIGURE 3. Schematic of explosively driven gradient shock tube used in experiments.

3. Experimental arrangement

A schematic diagram of the gradient shock tubes used in the experiments is shown in figure 3. The 10 cm diameter high explosive driver consists of a detonator, a plane wave generator and a 2·54 cm thick disk of perforated plastic bonded explosive (PBX 9404, giving ~ 1·6 megajoules of energy). The expanding explosive debris constitute the piston which drives a shock wave through section 1, which is filled with hydrogen at one atmosphere (~ 635 Torr at Albuquerque, New Mexico). A 10^{-3} in. mylar diaphragm separates the first 10 cm diameter lucite section from the second, which is initially evacuated until the air left is at a few millitorr. Two crossed 5×10^{-3} in. tungsten wires are fixed to the low pressure side of the diaphragm with spots of Mylar tape. The diaphragm is opened by exploding the wires with a capacitor discharge (5 kV, 21·0 mfd) prior to the arrival of the explosively driven shock at the diaphragm station. Rogowsky coils were used to monitor the wire current to obtain the current shut-off time, at which the diaphragm opens.

Framing and streak cameras were used to obtain photographs of visible luminous phenomena in the shock tube. An image of the shock tube axis was focused on the slit of the streak camera. The framing camera viewed the entire shock tube. Oscilloscopes were used to monitor the Rogowsky coil signals. The shock tube was destroyed in each test.

4. Results

Streak camera records from three experiments are shown in figure 4 (plate 1). The incident shock speeds S_I were 1·5 cm/μs. The acceleration of the shock through the gradient can be seen until the light fades out. This face-out is associated with the entry of the shock wave into the more tenuous region, where it is postulated that the flow becomes a high-speed free expansion. The collision of the high-speed expansion with the shock tube end wall is indicated by the intense light there.

Relevant data for the three experiments are shown in table 1. Note that lower transmitted speeds U_{EX} are associated with shorter times Δt between diaphragm

Experiment	Δt, μs	P_2, mtorr	U_{EX} cmμs^{-1}	Ambient gas Kn (region 2)
(*a*)	0	15·0	4·75	0·06
(*b*)	17	6·3	5·25	0·14
(*c*)	60	3·5	5·5	0·26

TABLE 1. Summary of experiments. Δt = time between initiation of discharge to diaphragm wires and the time when the detonation of the explosives is complete. The latter is time when the explosive debris begins to expand and drive a shock in region 1.

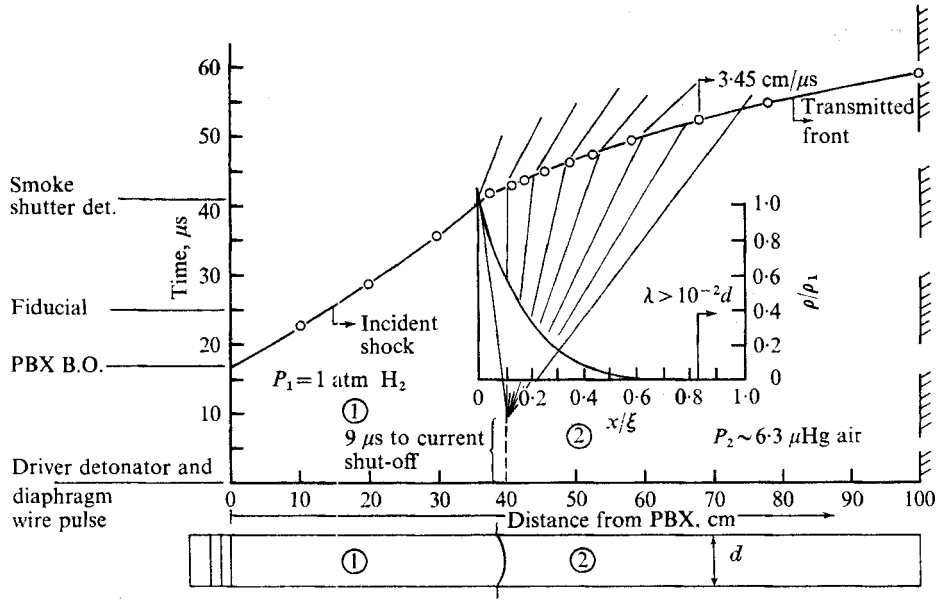

FIGURE 5. Explosively driven gradient shock tube experiment (*b*): data and theory. Line drawn by inspection through data points (○).

opening and launching of the incident shock in chamber 1. For larger values of Δt, the gradient has more time to stretch (longer ξ), providing a smoother transition from the high to low pressure region. The smoothness of the transition seems to be important even though the shape $d\rho/dx$ of the profile does not enter into the theory. This was exemplified by an experiment in which the diaphragm was not burst prior to shock arrival but was broken by the shock; the transmitted front speed was only 3·5 cm/μs with that abrupt transition in density.

Data from the streak camera record for experiment (*b*) are shown in figure 5 together with the calculated rarefaction wave density profile. With the high ambient gas Knudsen number in region 2, model 1 is expected to be valid only in the higher density regions of the rarefaction wave. For example, for $P_{12} \sim 10^4$, $Kn \sim 10^{-2}$, which corresponds to $x/\xi \sim 0{\cdot}84$, and with $M_I = S_I/a_1 = 11{\cdot}2$, where $a_1 = 0{\cdot}1324$ cm/μs from Gayden & Hurle (1963), model 1 gives a theoretical shock speed of 3·45 cm/μs. The measured shock speed corresponding to the above parameters was 3·45 cm/μs ± 5 %, in good agreement with theoretical predictions.

If a well-structured shock continued to propagate out of the rarefaction wave ($P_{12} > 10^5$), according to model 1 the final front speed should be $> 6{\cdot}9$ cm/μs. However, the measured transmitted front speed in region 2 was only $5{\cdot}25$ cm/μs $\pm 5\,\%$.

From the calculations by Gross (1967) a shock thickness for the region 2 pressures used would be the order of one metre, the diameter d of the shock tube being 10 cm. The flow boundary-layer thickness δ is proportional to the distance behind the leading edge of the shock and inversely proportional to the square root of the Reynolds number, i.e. $\delta = x/Re^{\frac{1}{2}} = x(\mu/ud)^{\frac{1}{2}}$. The coefficient of viscosity μ is obtained from the work of Turcotte & Scholnic (1969):

$$\mu = \tfrac{5}{16}(\pi mkT)^{\frac{1}{2}}/\pi\sigma^2,$$

where σ is the atomic diameter, k is Boltzmann's constant, m is the atomic mass and T is temperature. From these expressions it can be shown that for region 2 of our experiments the boundary layer envelopes the flow in a distance comparable with the shock thickness. We thus assume this shock thickness-to-tube diameter ratio in region 2 to be too great for a well-structured hydroshock to exist. In this paper we do not consider electrostatic collisionless shocks, nor do we consider the oblique case of magnetic collision shocks which might arise because of the oblique orientation of the earth's field with the shock tube axis in these experiments.

In region 2 we apply model 2. For $S_I = 1{\cdot}5$ cm/μs, $\gamma_1 = 1{\cdot}4$, $\gamma_5 = 1{\cdot}25$, as obtained from the real-gas calculations, and $T_5 = 4500\,^\circ$K, $T_1 = 300\,^\circ$K and $a_1 = 0{\cdot}1324$ cm/μs, equation (6) gives $U_{EX} = 5{\cdot}25$ cm/μs. Thus, the speed predicted by model 2 agrees with the measured value for the flow front velocity in region 2. Similar agreement was found for experiment (*c*). The results of experiment (*a*) were more than 10 per cent too low; this was attributed to (i) the inference from the studies that the gradient profile is physically important and (ii) the fact that the ambient pressure P_2 was more than twice that of experiments (*b*) and (*c*). Similar experiments have also been done with argon at one atmosphere in region 1, and it was found that (6) properly predicts the flow front speed in the high Knudsen number region.

Another qualitative observation can be made from figure 6 (plate 2), which is a framing camera photo sequence of experiment (*b*). In these pictures the intense luminosity of the incident front (left of the diaphragm location) is associated with the incident shocked gas and explosive debris. As the shock interacts with the gradient, another luminous region (just to the right of the diaphragm location) is seen to appear ahead of the main luminous region, and run ahead of it with increasing relative speed. This observation, substantiated by the streak camera record (figure 4, plate 1), is interpreted as showing the increasing separation of shock-heated hydrogen and explosive debris. This is to be expected since the gradient exerts a force on the gas and the molecular weight of hydrogen is considerably less than that of the explosive debris. In figure 6 the indicated shock front–explosive debris separation is approximately 25 cm at the time the high-speed expansion reaches the shock tube end wall. The separation would be considerably less ($\sim$ 10 cm) if no gradient acceleration were used.

5. Summary

The interaction of a strong shock with an ambient gas of decreasing density has been investigated both experimentally and theoretically, with empirical inclusion of real-gas effects, namely thermophysical properties, in the theory. For finite geometries and the case of high pre-shock Knudsen numbers it was postulated that the wall effects would degrade the shock structure and that in this case a shock-flow model would not be valid. A simple free-expansion model was presented to describe the flow front speed for high Knudsen numbers. Experimental results using explosively driven shock tubes with pre-shock density gradients produced by rarefaction waves verified both the shock-flow model for low Knudsen numbers and the free-expansion model for high Knudsen numbers.

The assistance of D. L. Cook in assembling the experiments, and W. P. Brooks, R. W. Olson and L. E. Heames in conducting the experiments at the explosives test site is gratefully acknowledged. The discussions with M. Cowan, and D. Compton of N.A.S.A., Ames were most helpful. This work was supported by the U.S. Atomic Energy Commission.

REFERENCES

FREEMAN, J. R. 1968 Equilibrium hydrodynamic variables behind incident and reflected shock waves in hydrogen. *Sandia Laboratories, Albuquerque Rep.* SC-RR-68-687.

GAYDON, A. G. & HURLE, I. R. 1963 *The Shock Tube in High Temperature Chemical Physics.* New York: Reinhold.

GLASS, I. I. & HALL, J. G. 1959 Handbook of supersonic aerodynamics, section 18: shock tubes. *NAVORD Rep.* no. 1488.

GOULD, D. G. 1952 The head-on collision of two shock waves and a shock and rarefaction wave in one-dimensional flow. *University of Toronto, U.T.I.A. Rep.* no. 7.

GREENSPAN, H. P. & BUTLER, D. S. 1962 On the expansion of gas into vacuum. *J. Fluid Mech.* **13**, 101–119.

GROSS, R. A. 1967 Thickness of a shock wave in hydrogen. *Phys. Fluids*, **10**, 1853–1855.

GUREVICH, L. E. & RUMYANTSEV, A. A. 1970 Propagation of shock waves in a medium of decreasing density. *Soviet Phys. J.E.T.P.* **31**, 747–749.

MCDANIEL, E. W. 1964 *Collision Phenomena in Ionized Gases.* Wiley.

MIRELS, H. 1963 Test time in low-pressure shock tubes. *Phys. Fluids*, **6**, 1201–1214.

NICHOLL, C. I. H. 1951 The head-on collision of shock and rarefaction waves. *University of Toronto, U.T.I.A. Rep.* no. 10.

STEFANIK, R. P. 1969 The propagation of shock waves in non-uniform media. *Air Force Camb. (Mass.) Res. Lab. Rep.* 69-0180. (Available from *Center for Sci. Tech. Inf. Washington*: AD 691836.)

STRACHAN, J. O., HUNI, J. P. & AHLBORN, B. 1970 Shock propagation into inhomogeneous media. *J. Fluid Mech.* **43**, 487–496.

TURCOTTE, D. L. & SCHOLNICK, I. M. 1969 Structure of strong shock waves. *Phys. Fluids*, **12** (suppl. I), 79–82.

ZELDOVICH, YA. B. & RAIZER, YU. P. 1967 *Physics of Shock Waves and High Temperature Hydrodynamic Phenomena.* Academic.

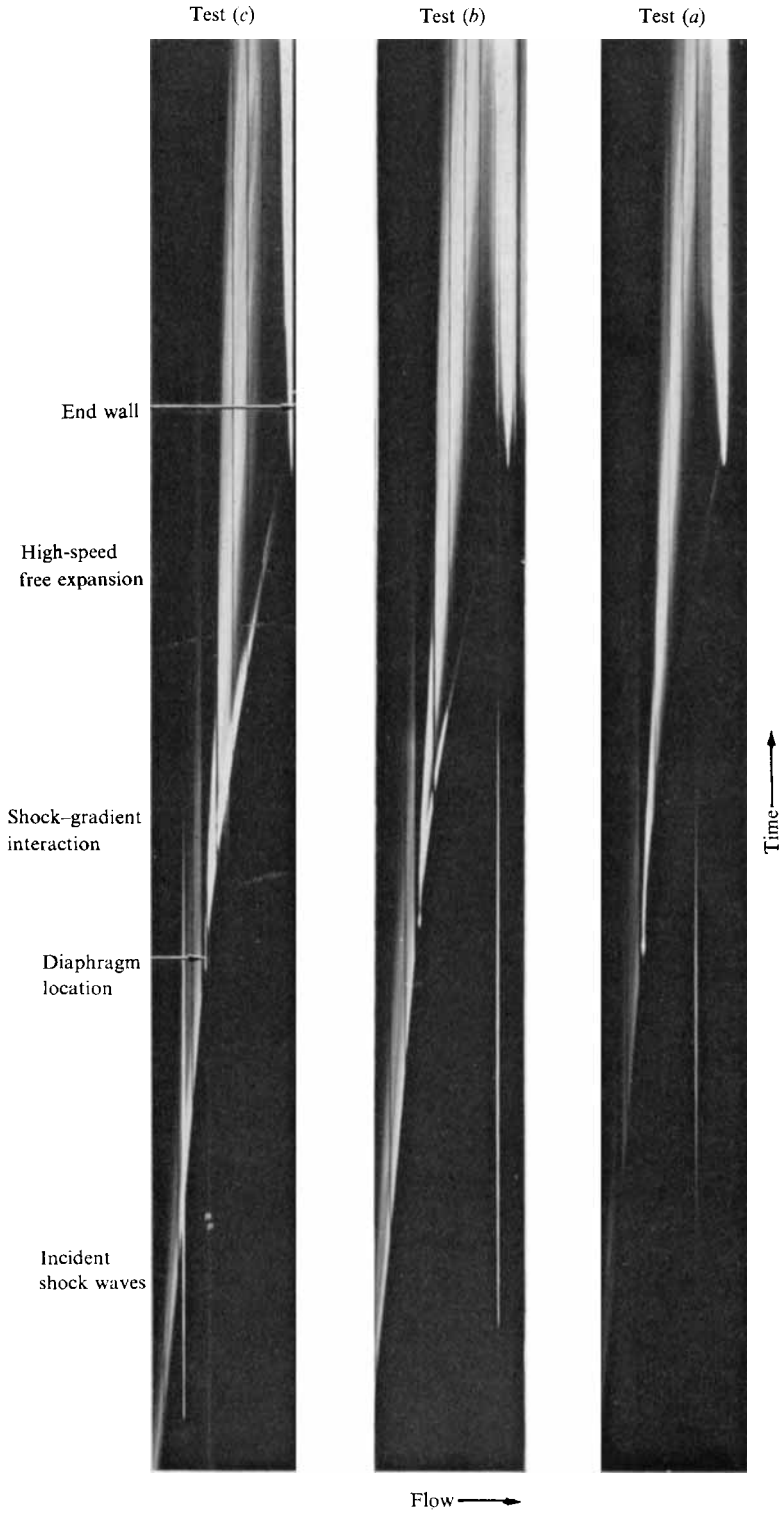

FIGURE 4. Streak camera photographs of three gradient shock tube tests.

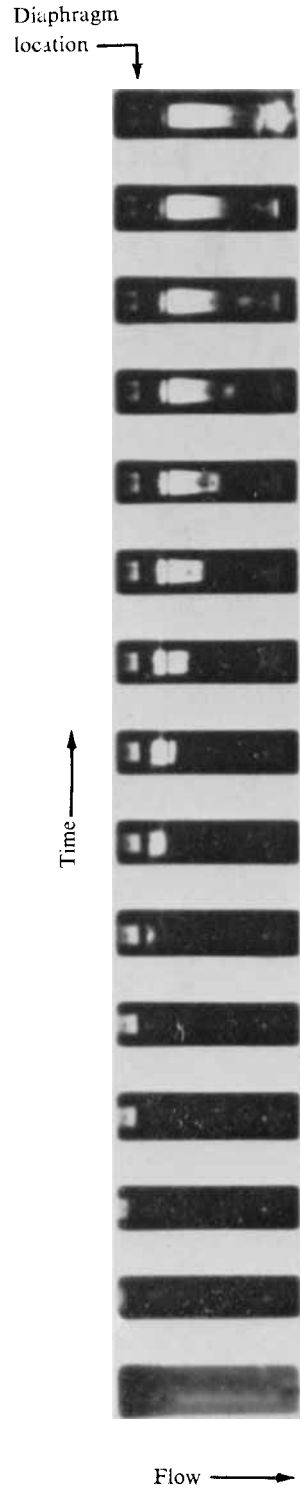

FIGURE 6. Framing camera photographs of experiment (*b*), 2·0 μs per frame.